ACS APPLIED ENERGY MATERIALS

www.acsaem.org

Article

Solar Harvesting Efficiency of Janus M_2CTT'(M = Y, Sc; T/T′ = Br, Cl, F) MXene Monolayers for Photovoltaic Applications

Bill D. Aparicio-Huacarpuma,* Marcelo Lopes Pereira Júnior, Alysson M. A. Silva, Alexandre C. Dias, and Luiz Antônio Ribeiro Júnior*

Cite This: ACS Appl. Energy Mater. 2025, 8, 6634−6644

Read Online

ACCESS | Metrics & More | Article Recommendations | Supporting Information

ABSTRACT: Two-dimensional (2D) Janus MXene monolayers have emerged as promising candidates for photovoltaic and optoelectronic applications due to their highly tunable physicochemical properties, which enable optimized light absorption and enhanced power conversion efficiency (PCE). In this study, we investigate the structural, electronic, excitonic, and optical properties of 2D Janus MXenes with the general formula M_2CTT' (M = Sc, Y; TT′ = FCl, FBr, ClBr) using density functional theory calculations combined with a semiempirical tight-binding approach. All six monolayers are found to be structurally stable, exhibiting a trigonal configuration with cohesive energies ranging from −5.74 eV/atom to −5.22 eV/atom. Their electronic band structures reveal an indirect semiconducting nature, with band gaps spanning 1.63 to 1.83 eV. The computed linear optical properties indicate strong absorption in the visible, infrared, and ultraviolet regions, reinforcing their potential for solar energy harvesting. Strong many-body effects are observed, with exciton binding energies between 249 and 373 meV, which are crucial for accurately describing energy conversion processes. The estimated PCE, evaluated using both the Shockley−Queisser (SQ) limit and the pectroscopy-limited maximum efficiency (SLME) approach, ranges from 25.5% to 32.6%, positioning these Janus M_2CTT' MXenes as strong contenders for next-generation photovoltaic devices.

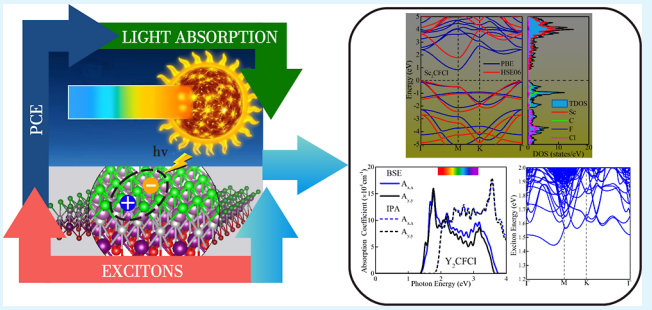

KEYWORDS: *Janus MXenes, photovoltaics, optoelectronic properties, excitonic effects, power conversion efficiency*

1. INTRODUCTION

Two-dimensional (2D) transition metal carbides and nitrides, commonly referred to as MXenes,[1] have garnered considerable interest in theoretical research due to their exceptional properties and high tunability. MXenes are typically synthesized through the exfoliation of MAX phases,[2] where M denotes an early transition metal,[3,4] A is an element from groups 13 or 14 of the periodic table,[5] and X corresponds to either carbon or nitrogen.

These compounds are generally described by the formula $M_{n+1}X_n$ and can be functionalized with surface groups such as F, OH, O, or other elements from groups 16 and 17.[1] The extended chemical formula, $M_{n+1}X_nT_x$ (n = 1, 2, 3, or 4), accounts for these surface terminations,[6,7] where T_x denotes the set of functional groups attached to the outer layers of the MXene structure.

MXenes can also exhibit dual surface functionalization, as observed in compounds such as M_2CTT'[8] or in carbide frameworks composed of two distinct metals, exemplified by $MM'CT_2$.[9] The emergence of Janus 2D materials, characterized by asymmetric atomic terminations on opposing surfaces, has further expanded the possibilities for engineering atomically tailored systems. These Janus monolayers exhibit distinct physicochemical properties from their nanoscale dual-surface architecture, making them promising candidates for various technological applications.[10]

For instance, Bernardi et al. laid the groundwork for applying semiconducting monolayers in photovoltaics, emphasizing the tunability of their properties through compositional adjustments and domain structure engineering.[11] Their work demonstrated that even ultrathin materials, such as bilayer CBN, can achieve significant solar energy conversion efficiency, thereby motivating further investigations into 2D materials for solar harvesting applications.

Building on this, Wei et al. investigated photodetectors based on transition metal dichalcogenide (TMD) heterostructures, showing that the integration of TMDs with graphene electrodes can significantly enhance photocurrent response in field-effect transistors (FETs).[12] In parallel,

Received: March 7, 2025
Revised: May 5, 2025
Accepted: May 8, 2025
Published: May 15, 2025

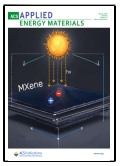

https://doi.org/10.1021/acsaem.5c00657
ACS Appl. Energy Mater. 2025, 8, 6634−6644

Khazaei et al. emphasized the electronic, optical, and electrochemical versatility of MXenes, underlining their suitability for energy conversion applications due to their highly tunable characteristics.[2,13]

Recently, Xiong et al. investigated the transport properties of Janus MXenes with the $MM'CT_2$ configuration, reporting band gaps in the range of 1.34−1.94 eV and high carrier mobilities, suggesting their suitability for visible-light applications.[14] Wong and collaborators explored asymmetrically ordered Janus MXene alloys, such as $TiMoCO_2$, using first-principles simulations, cluster expansion, and Monte Carlo methods. Their results demonstrated the potential of these systems for photocatalytic water splitting and thermoelectric applications.[15]

Sibhatu's group focused on hexagonal van der Waals heterostructures composed of $MX_{2/t}ZrXO$ (where M = W, Mo, and X = S, Se), highlighting their strong absorption in the visible-to-ultraviolet range and high energy conversion efficiencies, making them promising candidates for photovoltaic devices.[16]

Similarly, silicon−transition metal clusters (MSi_n), incorporating various metallic elements, have been investigated over the past few decades for their potential to form crystalline phases, which could act as conductive components in self-assembled nanodevices.[17,18]

Alhamada and coauthors investigated the integration of MXenes into photovoltaic (PV) cells, reporting notable enhancements in operational stability and power conversion efficiency.[19] In parallel, several comprehensive reviews have highlighted the rapid progress in MXene research and its wide-ranging applications in energy conversion, electronics, and catalysis.[20−23]

Despite these significant advancements, studies specifically focused on Janus MXenes of the form Sc_2CTT' and Y_2CTT', featuring asymmetric surface terminations ($T \neq T'$; e.g., F, Cl, Br), remain scarce in the literature. This gap underscores the need for a detailed investigation of their structural, electronic, and optoelectronic properties.

Zhang et al. systematically investigated Janus-functionalized Sc_2CTT' MXenes, focusing on configurations such as Sc_2COHCl, Sc_2CHCl, and Sc_2CFCl, and explored their structural, electronic, and optical properties.[10] Their findings revealed promising applications in spintronics, photocatalysis, and solar energy conversion with high power conversion efficiencies and notable absorption in the infrared region.

Modi and coauthors examined Y_2CTT' monolayers functionalized with halides (F, Cl, Br), highlighting their electronic and optical characteristics. These structures were identified as indirect band gap semiconductors exhibiting strong absorption in the ultraviolet region, making them suitable candidates for photonic and optoelectronic applications.[8]

While these studies have laid an essential foundation, a comprehensive evaluation of excitonic effects and their influence on the linear optical response of Sc_2CTT' and Y_2CTT' systems remains lacking, particularly in the context of photovoltaic applications.

In this work, we explore the structural, electronic, and optical properties of MXene monolayers with the general formula Sc_2CTT' and Y_2CTT', with particular emphasis on excitonic effects and their influence on optical behavior. Our analysis is based on first-principles calculations within the density functional theory (DFT) framework, complemented by a semiempirical approach using the maximally localized Wannier function tight-binding model (MLWF-TB).

The selection of these systems was informed by data from the MXene database (https://anant.mrc.iisc.ac.in/apps/mxene), where compounds containing Sc and Y were found to exhibit band gaps in the range suitable for solar energy harvesting. Guided by this, we constructed the Janus monolayers investigated in this study using those database compounds as structural and electronic references.

Our results reveal that these monolayers exhibit favorable electronic structures and strong optical absorption in the visible and infrared regions, establishing their potential for applications in nanoelectronics and photovoltaics. Moreover, the estimated power conversion efficiencies ranging from 25.5% to 32.6% further reinforce their promise as next-generation materials for solar energy technologies.

2. METHODOLOGY

The structural optimization and electronic properties of the Janus MXenes were calculated using the Vienna Ab initio Simulation Package (VASP),[24,25] within the framework of density functional theory (DFT),[26,27] and employing the projector augmented-wave (PAW) method.[28,29] The Perdew−Burke−Ernzerhof (PBE) exchange−correlation functional[30,31] was used for structural optimization, phonon dispersion, and electronic structure calculations. A plane-wave cutoff energy of 800 eV was adopted to ensure the numerical accuracy.

The Brillouin zone was sampled using Monkhorst−Pack grids of 12 × 12 × 1 and 14 × 14 × 1 for structural relaxation, and 24 × 24 × 1 and 28 × 28 × 1 for band structure and density of states calculations, for Y_2CTT' and Sc_2CTT', respectively. To avoid spurious interactions between periodic images, vacuum layers of 25 Å and 28 Å were introduced along the z-direction for Y_2CTT' and Sc_2CTT', respectively. Convergence criteria of 1×10^{-6} eV for the self-consistent total energy and 0.01 eV $Å^{-1}$ for residual atomic forces were applied during structural optimization.

To address the well-known underestimation of band gaps by the PBE functional,[32,33] the hybrid Heyd−Scuseria−Ernzerhof (HSE06) functional[34] was employed for band structure corrections, following recommendations from the literature.[33,35] Structural visualization and analysis were carried out using the VESTA software,[36] while VASPKIT[37] was used for postprocessing. Phonon dispersion calculations were performed using density functional perturbation theory (DFPT) as implemented in the Phonopy package,[38] in combination with VASP (PBE functional), using 2 × 2 × 1 supercells and the same k-point density as employed for the electronic structure.

Maximally localized Wannier functions were generated using the Wannier90 code[39] to construct tight-binding (TB) Hamiltonians directly from HSE06-calculated electronic states.

Excitonic and optical properties were computed using the WanTiBEXOS code.[40] The orbital projections included d-orbitals for Sc and Y, and p-orbitals for C, F, Cl, and Br. Optical spectra were evaluated within the independent-particle approximation (IPA), excluding excitonic effects, and at the Bethe−Salpeter equation (BSE) level, incorporating electron−hole interactions. A k-point density of 120 $Å^{-1}$ in the 2D plane was used for optical calculations. The BSE calculations employed a 2D truncated Coulomb interaction (V2DT)[41] to properly account for dimensionality effects. Dielectric functions were obtained using Gaussian smearing of 0.05 eV,

https://doi.org/10.1021/acsaem.5c00657
ACS Appl. Energy Mater. 2025, 8, 6634−6644

considering the lowest conduction band and the top three valence bands.

The power conversion efficiency (PCE) was evaluated using WanTiBEXOS, based on both the Shockley−Queisser (SQ) limit[42] and the spectroscopy-limited maximum efficiency (SLME) model.[43] Unlike the SQ limit, which requires only the band gap (or the exciton ground state when quasi-particle corrections are included), the SLME approach also considers the band gap's nature (direct/indirect) and the material's absorption coefficient. The AM1.5G solar spectrum[44,45] was used, assuming an operational temperature of 300 K.

The absorbance was calculated from the total absorption coefficient and system thickness using diagonal components of the dielectric function. Monolayer thickness was defined as the intrinsic thickness of the material plus a van der Waals (vdW) correction of 3.21 Å, following the approach proposed by Bernardi et al.,[45] which has been validated for graphene and other 2D systems, yielding results consistent with experimental observations.

3. RESULTS

3.1. Structural and Mechanical Properties. Figure 1 presents the top and side views of the Janus-like M_2CTT' (M = Sc, Y; T, T′ = FCl, FBr, ClBr) MXene monolayers. These systems adopt a trigonal crystal structure (space group $P3m1$), characterized by lattice angles $\alpha = \beta = 90°$ and $\gamma = 120°$ and are modeled under periodic boundary conditions in the xy plane.

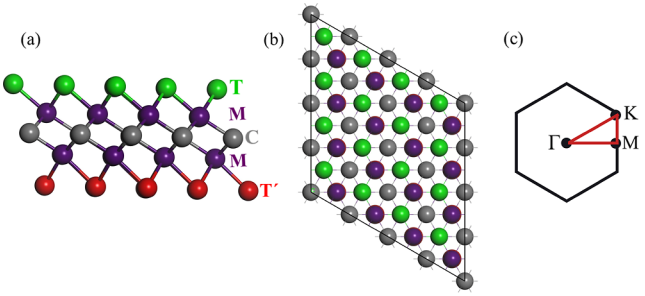

Figure 1. Side (a) and top (b) views of M_2CTT' Janus-like MXene monolayers. (c) Representation of the first Brillouin zone derived from the crystal structure. The atomic layers follow a T−M−C−M−T′ stacking configuration, where M represents Sc or Y atoms, C denotes carbon, and T, T′ are functional groups (F, Cl, Br).

Structurally, each monolayer consists of five atomic layers arranged in a T−M−C−M−T′ stacking sequence, where M corresponds to transition metals (Sc or Y), C represents the carbon layer, and T/T′ indicates surface terminations composed of halogen atoms (F, Cl, Br). From these configurations, six distinct Janus monolayers were constructed: Sc_2CClBr, Sc_2CFBr, Sc_2CFCl, Y_2CClBr, Y_2CFBr, and Y_2CFCl.

Optimized lattice parameters (a_0) for the six Janus monolayers were obtained using the PBE functional and are summarized in Table 1. The values show excellent agreement with previous reports in the literature.[8,10] In addition to the lattice constants, Table 1 includes the adequate monolayer thickness (defined as the geometric thickness plus a van der Waals correction, t_0) and the cohesive energy (E_{coh}), calculated as

Table 1. Cohesive Energy (E_{coh}), Optimized Lattice Parameter (a_0), and Monolayer Thickness Added with van der Waals Length (t_0) for the Investigated Janus-like MXenes, Compared with Published Results

Janus-like MXene	E_{coh} (eV/atom)	a_0 (Å)	t_0 (Å)
Sc_2CClBr	−5.216	3.48	9.16
Sc_2CFBr	−5.566	3.40	8.66
Sc_2CFCl	−5.732	3.36 (3.34[10])	8.52
Y_2CClBr	−5.261	3.74 (3.72[8])	9.56
Y_2CFBr	−5.600	3.67 (3.64[8])	9.02
Y_2CFCl	−5.741	3.64 (3.62[8])	8.85

$$E_{coh} = \frac{E_{tot}(M_2CTT') - (\sum_{i=M,C,T,T'} N(i)E(i))}{N(M_2CTT')} \quad (1)$$

where $E_{tot}(M_2CTT')$ is the total energy of the Janus MXene unit cell, $E(i)$ is the energy of the isolated atom i, and $N(i)$ is the number of atoms of type i in the unit cell. Specifically, $N(M) = 2$ for transition metals (M = Sc, Y), and $N(C) = N(T) = N(T') = 1$ for carbon and surface terminations (T, T′ = F, Cl, Br). The denominator $N(M_2CTT')$ represents the total number of atoms in the monolayer.

A clear correlation is observed between the optimized lattice parameter (a_0) and the atomic radius of the functional groups in the Janus MXene structures. For Sc-based monolayers, a_0 increases from 3.36 Å to 3.48 Å across the FCl, FBr, and ClBr configurations, respectively, reflecting the progressive enlargement of the terminating atoms. A similar trend is found in the Y-based systems, with a_0 ranging from 3.64 Å (FCl) to 3.74 Å (ClBr).

This expansion in lattice parameter is accompanied by an increase in monolayer thickness (t_0), which spans from 8.52 Å to 9.16 Å for Sc-based systems and from 8.85 Å to 9.56 Å for those based on Y, in agreement with prior studies.[8,10]

Cohesive energy (E_{coh}) analysis reveals distinct stability trends among the configurations. The M_2CClBr structures exhibit lower stability in comparison to those functionalized with FCl. Overall, E_{coh} values range from −5.216 eV/atom for Sc_2CClBr to −5.741 eV/atom for Y_2CFCl, the most stable compound in the set. In general, Y-based monolayers tend to display cohesive energies slightly lower than those of their Sc-based counterparts. Regarding functionalization, the combinations ClBr, FBr, and FCl yield approximate cohesive energies of −5.2 eV/atom, −5.6 eV/atom, and −5.7 eV/atom, respectively, for both families of Janus-like MXenes.

Dynamic stability was assessed through phonon dispersion calculations along the Γ−M−K−Γ high-symmetry path, as shown in Figure 2. A material is dynamically stable when no imaginary frequencies (plotted as negative values) appear in its phonon spectrum. However, since these frequencies are obtained numerically, minimal imaginary values, especially those near the Γ point, can often be attributed to numerical artifacts.

Among the studied systems, Figure 2(a) and (c) exhibits no imaginary frequencies, confirming the dynamical stability of the Sc_2CFCl and Y_2CFCl monolayers. In contrast, Figure 2b−f displays small imaginary modes with magnitudes lower than −1 THz, located near the Γ point. These minor anomalies are likely the result of numerical error propagation and do not indicate physical instability. Therefore, all systems can be regarded as dynamically stable.

https://doi.org/10.1021/acsaem.5c00657
ACS Appl. Energy Mater. 2025, 8, 6634−6644

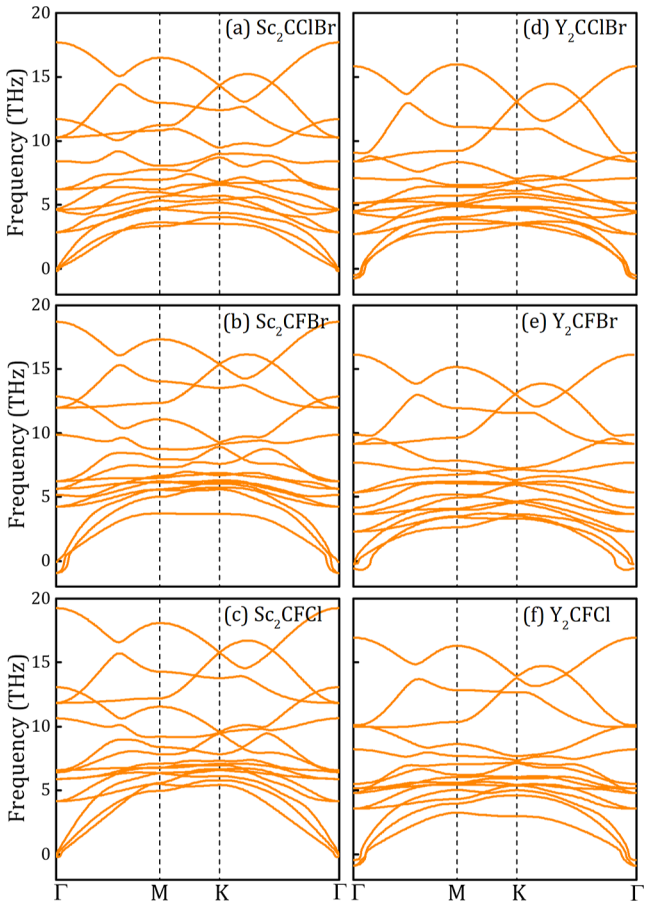

Figure 2. Phonon spectra of (a) Sc_2CClBr, (b) Sc_2CFBr, (c) Sc_2CFCl, (d) Y_2CClBr, (e) Y_2CFBr, and (f) Y_2CFCl Janus MXene monolayers.

Additionally, the maximum phonon frequencies for the monolayers Sc_2CClBr, Sc_2CFBr, Sc_2CFCl, Y_2CClBr, Y_2CFBr, and Y_2CFCl are found to be 17.69 THz (~590 cm^{-1}), 18.70 THz (~624 cm^{-1}), 19.26 THz (~642 cm^{-1}), 15.85 THz (~529 cm^{-1}), 16.13 THz (~538 cm^{-1}), and 16.95 THz (~565 cm^{-1}), respectively, indicating robust vibrational behavior across all configurations.

Thermodynamic potentials were also assessed via density functional perturbation theory (DFPT), allowing the computation of Gibbs free energy $F(T)$, entropy $S(T)$, and heat capacity C_v as functions of temperature (in K). The results, shown in the Supporting Information (Figures S1−S3), demonstrate that all monolayers exhibit favorable Gibbs free energy behavior at temperatures above 200 K, in line with trends observed in entropy and heat capacity. These findings indicate that Janus MXenes are thermodynamically stable under typical synthesis conditions, further reinforcing their experimental viability.

Mechanical stability was further evaluated by computing the elastic constants of each Janus-like M_2CTT' monolayer (M = Sc, Y; T, T′ = FCl, FBr, ClBr). According to the Born−Huang stability criteria,[46] a 2D material is mechanically stable when $C_{11}C_{22}-C_{12}^2 > 0$ and $C_{66} > 0$. Owing to the symmetry of the monolayers, it holds that $C_{11} = C_{22}$ and $C_{66} = (C_{11} - C_{12})/2$.

The computed elastic constants C_{ij} are listed in Table 2 and confirm that all structures satisfy the aforementioned mechanical stability conditions.

Table 2. Elastic Constants C_{ij} (N/m), Maximun Young's Modulus Y_{max}, and Maximum Poisson's Ratio ν_{max}[a]

system	C_{11} (N/m)	C_{22} (N/m)	C_{12} (N/m)	C_{66} (N/m)	Y_{max} (N/m)	max
Sc_2CClBr	143.76	143.76	35.86	53.96	134.82	0.25
Sc_2CFBr	157.28	157.28	37.55	59.88	148.34	0.24
Sc_2CFCl	157.79	157.79	36.23	60.73	149.47	0.23
Y_2CClBr	116.50	116.50	27.47	44.28	110.02	0.24
Y_2CFBr	133.03	133.03	33.11	48.76	124.79	0.25
Y_2CFCl	132.67	132.67	32.33	49.99	124.79	0.24

[a]The Young's modulus is in units of N/m, while Poisson's ratio is dimensionless.

When simulating 2D materials, it is essential to introduce a vacuum layer along the nonperiodic direction to eliminate spurious interactions between periodic images of the monolayer. This consideration is critical in plane-wave-based calculations, where the system is periodic in all three spatial directions. To ensure that the elastic constants are independent of the vacuum size, their values, originally in GPa (or N/m^2), were converted to units of N/m by multiplying by the vacuum thickness (in meters).

From the computed elastic coefficients, we derived the Young's modulus (Y) and Poisson's ratio (ν) for each structure, following the methodology described by Amirian et al.[47] As shown in Figure S10, both Y and ν exhibit isotropic behavior across all Janus M_2CTT' monolayers (M = Sc, Y; TT′ = FCl, FBr, ClBr), consistent with the symmetry of the structures.[48]

The maximum Young's modulus values for the Sc-based monolayers decrease in the following order: Sc_2CFCl (149.47 N/m) > Sc_2CFBr (148.34 N/m) > Sc_2CClBr (134.83 N/m). A similar trend is observed for the Y-based systems: Y_2CFCl = Y_2CFBr (124.79 N/m) > Y_2CClBr (110.02 N/m). In general, the Y-based monolayers display a lower stiffness than their scandium counterparts.

These findings are in good agreement with previous reports. In particular, Young's modulus of Sc_2CTT' systems is significantly higher than that of pristine Sc_2C,[49] and a similar enhancement is observed for functionalized Y_2CTT' systems compared to the unfunctionalized Y_2C monolayer.[50]

As for the Poisson's ratio, the computed maximum values for Sc_2CClBr, Sc_2CFBr, Sc_2CFCl, Y_2CClBr, Y_2CFBr, and Y_2CFCl are 0.25, 0.24, 0.23, 0.24, 0.26, and 0.25, respectively. These values place the Janus monolayers at the threshold between ductile and brittle regimes, with a slight tendency toward brittle behavior.[51] For comparison, nonfunctionalized MXenes such as Sc_2C and Y_2C exhibit significantly lower Poisson's ratios (around 0.1), indicating a more pronounced brittle character.[49,50]

3.2. Electronic Properties. Electronic band structures for the six Janus MXene monolayers were obtained by using both the PBE and HSE06 exchange−correlation functionals. Calculations were carried out along the high-symmetry path Γ−M−K−Γ in the Brillouin zone, reflecting the hexagonal symmetry of these systems, with the Γ point positioned at the center (see Figure 1c).

Results confirm that all structures exhibit semiconducting behavior. Each monolayer displays an indirect band gap, with the valence band maximum (VBM) located at the Γ point and the conduction band minimum (CBM) at the M point, as shown in Figure 3a,c,e,g,i,k.

https://doi.org/10.1021/acsaem.5c00657
ACS Appl. Energy Mater. 2025, 8, 6634−6644

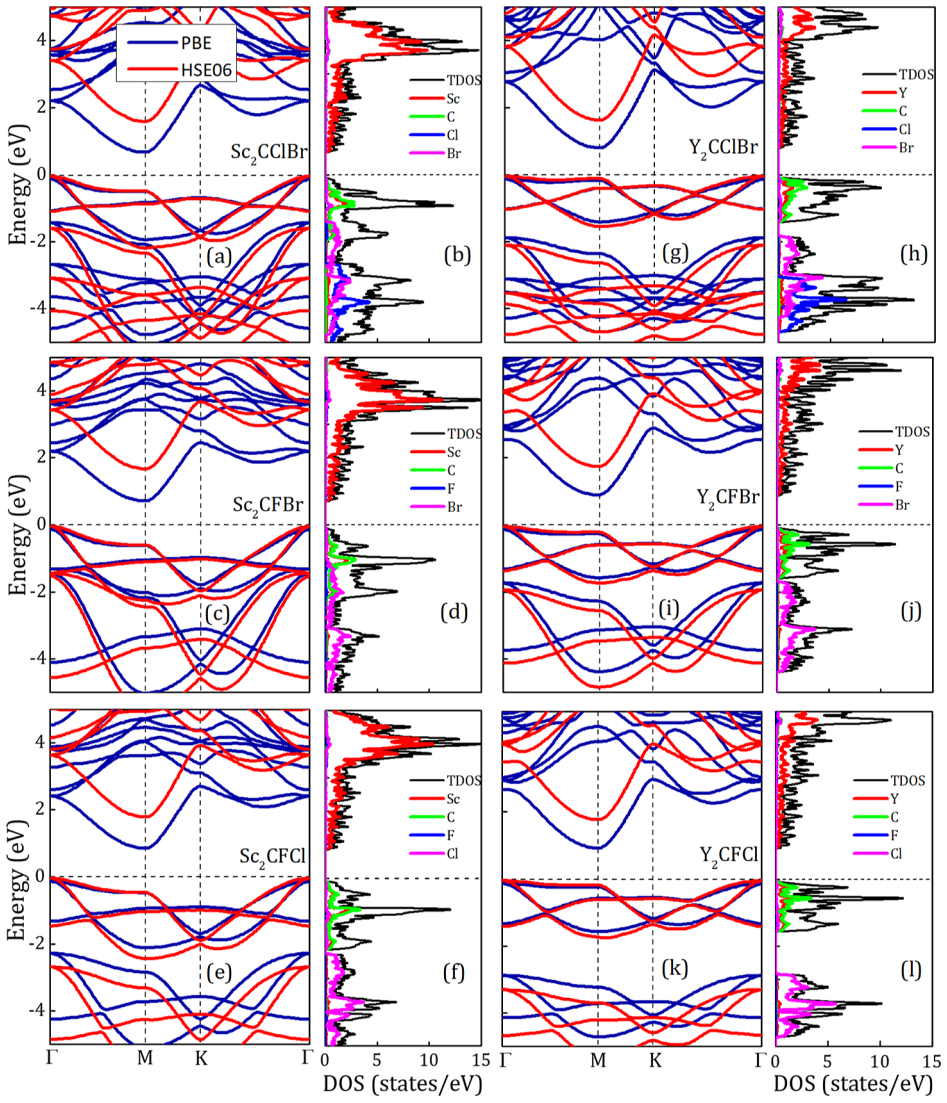

Figure 3. Electronic band structures and PDOS for the six Janus MXene monolayers. Panels (a), (c), (e), (g), (i), and (k) show the electronic band structures of Sc_2CClBr, Sc_2CFBr, Sc_2CFCl, Y_2CClBr, Y_2CFBr, and Y_2CFCl, respectively, calculated using the PBE (blue curves) and HSE06 (red curves) methods. Panels (b), (d), (f), (h), (j), and (l) display the corresponding PDOS for each system, highlighting the contributions of different atomic species to the electronic states near the Fermi level (set at 0 eV).

Since band gap values play a critical role in solar energy harvesting, semiconductors with gaps in the optimal range are particularly attractive due to their enhanced optical absorption.[52] To improve the accuracy of the band gap predictions, the HSE06 hybrid functional was employed in addition to PBE, addressing the known limitations of the conventional GGA approaches. A comparison of the electronic band gaps calculated with both methods is provided in Table 3.

As shown in Figure 3 and summarized in Table 3, the electronic band gaps computed with the PBE functional are 0.80 eV, 0.84 eV, and 0.98 eV for Sc_2CClBr, Sc_2CFBr, and Sc_2CFCl, respectively, and 0.93 eV, 1.03 eV, and 1.06 eV for Y_2CClBr, Y_2CFBr, and Y_2CFCl. These results, represented by the blue curves in Figure 3, agree with the values reported in the literature.[8]

Upon use of the HSE06 hybrid functional, a notable increase in the band gap is observed for all systems. The values rise to 1.63 eV, 1.71 eV, and 1.83 eV for the Sc-based structures and to 1.67 eV, 1.79 eV, and 1.82 eV for the Y-based monolayers, as indicated by the red curves in Figure 3.

Table 3. Comparison between PBE (E_g^{PBE}) and HSE06 (E_g^{HSE06}) Electronic Band Gaps of the Janus-like MXenes with Results of Published Data (E_g^{PBE})

Janus-like MXene	E_g^{PBE} (eV)	E_g^{HSE06} (eV)
Sc_2CClBr	0.80	1.63
Sc_2CFBr	0.84	1.71
Sc_2CFCl	0.98	1.83
Y_2CClBr	0.93 (0.95[8])	1.67
Y_2CFBr	1.03 (0.99[8])	1.79
Y_2CFCl	1.06 (1.04[8])	1.82

Interestingly, despite the difference in transition metal species, the band gap values for a given surface functionalization remain close, suggesting that the TT′ terminations dominate in determining the gap magnitude. The trend follows the order FCl > FBr > ClBr, indicating that lighter and more electronegative terminations lead to wider gaps. This behavior contrasts with the trend in the lattice constant, which

https://doi.org/10.1021/acsaem.5c00657
ACS Appl. Energy Mater. 2025, 8, 6634−6644

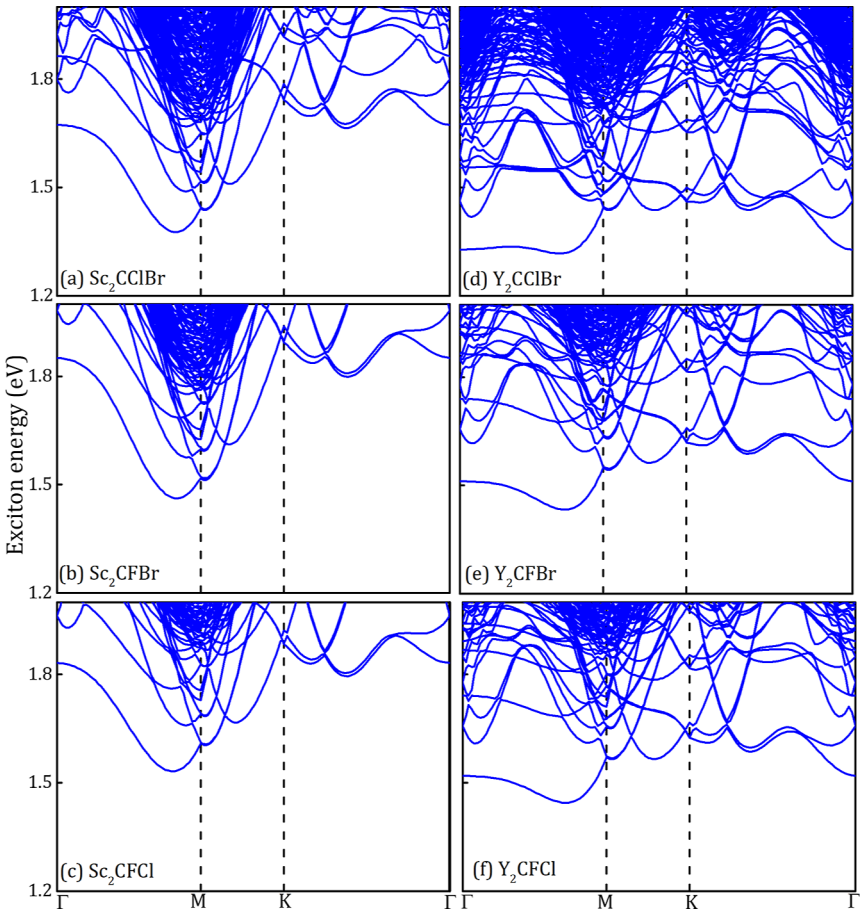

Figure 4. Exciton band structure of (a) Sc_2CClBr, (b) Sc_2CFBr, (c) Sc_2CFCl, (d) Y_2CClBr, (e) Y_2CFBr, and (f) Y_2CFCl Janus MXene monolayers.

increases in the opposite direction, implying that smaller lattice constants may be associated with larger band gaps.

In addition to the band structure analysis, the projected density of states (PDOS) was computed for all six Janus monolayers, as illustrated in Figure 3b,d,f,h,j,l. For the Sc_2CClBr, Sc_2CFBr, and Sc_2CFCl systems, the conduction band edge is primarily composed of Sc d-orbitals, accompanied by modest contributions from the p-orbitals of C, Cl, F, and Br, depending on the functional group. In contrast, the valence band edge is largely dominated by the p-orbitals of the same elements, with additional influence from Sc p−d hybridization.

A similar orbital character is observed in the Y_2CClBr, Y_2CFBr, and Y_2CFCl monolayers. The conduction band edge mainly arises from Y d-orbitals, with secondary contributions from C p-orbitals. The valence band is composed of p−d hybridized states from C, Cl, and Br, while F p-orbitals contribute more weakly in fluorinated systems.

Overall, these results highlight the strong dependence of the electronic structure on the chemical functionalization of the Janus MXenes. The tunability provided by surface terminations can be strategically exploited for optoelectronic and photovoltaic technologies applications.

3.3. Excitonic and Optical Properties. Excitonic quasiparticle effects in the Janus MXene monolayers were investigated by using the Bethe−Salpeter equation (BSE) formalism. As shown in Figure 4, the computed exciton band structures reveal that the excitonic ground state is indirect for all six configurations, regardless of their chemical composition. These transitions occur predominantly along the Γ−M path in systems functionalized with Cl, Br, and F.

This behavior is consistent with the indirect nature of the electronic band gap and suggests phonon-assisted optical transitions. As a result, optical excitations may occur at energies below the direct optical band gap, which is typically obtained by considering only vertical (momentum-conserving) transitions.

Table 4 summarizes the exciton binding energies (E_b) of the Janus MXene monolayers, defined as the difference between the fundamental electronic band gap (E_g) and the exciton ground state energy (Ex_{gs}), as obtained from the excitonic band structures shown in Figure 4. This parameter plays a crucial role in characterizing the optical response of two-

Table 4. Excitonic Properties Obtained with the MLWF-TB + BSE Method (HSE06 Parameterization): Fundamental Band Gap, E_g (eV), Direct Band Gap, E_g^d (eV), Exciton Ground State, Ex_{gs} (eV), Direct Exciton Ground State, Ex_{gs}^d (eV), and Exciton Binding Energy, Ex_b (eV), Calculated as $E_g - Ex_{gs}$

system	E_g (eV)	E_g^d (eV)	Ex_{gs} (eV)	Ex_{gs}^d (eV)	Ex_b (meV)
Sc_2CClBr	1.63	2.08	1.37	1.67	254.29
Sc_2CFBr	1.71	2.28	1.46	1.85	249.47
Sc_2CFCl	1.83	2.26	1.53	1.83	295.48
Y_2CClBr	1.67	1.75	1.32	1.33	357.05
Y_2CFBr	1.79	1.96	1.43	1.51	356.15
Y_2CFCl	1.82	1.66	1.44	1.52	372.64

https://doi.org/10.1021/acsaem.5c00657
ACS Appl. Energy Mater. 2025, 8, 6634−6644

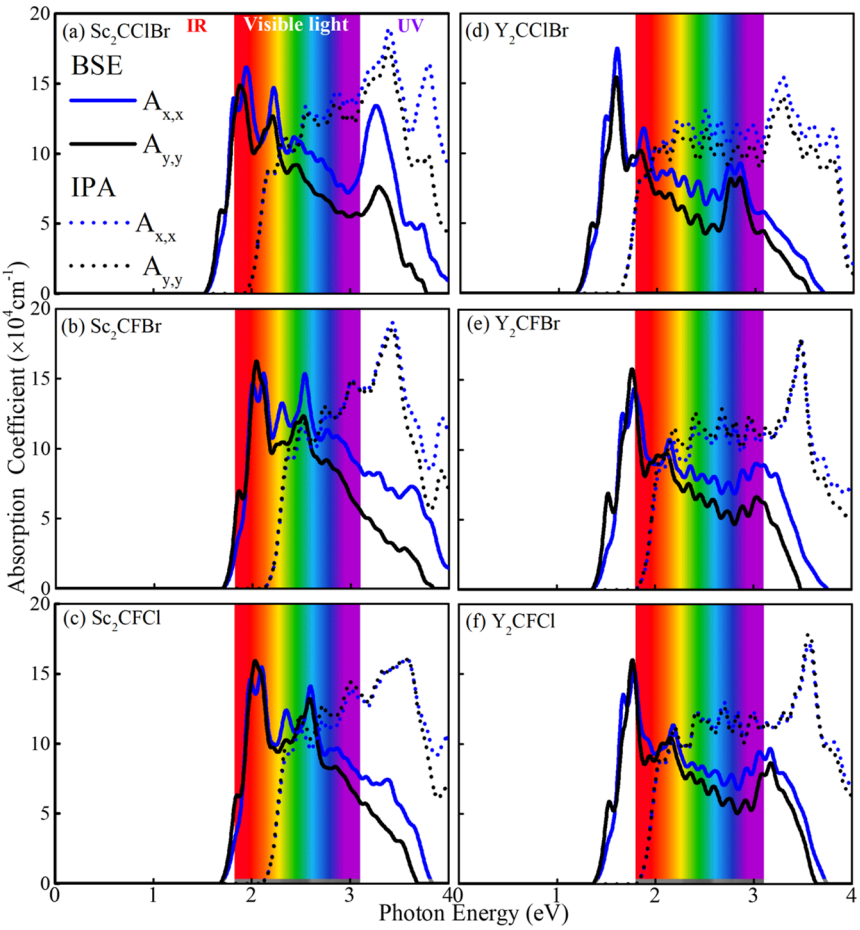

Figure 5. Optical absorption coefficient spectra of (a) Sc_2CClBr, (b) Sc_2CFBr, (c) Sc_2CFCl, (d) Y_2CClBr, (e) Y_2CFBr, and (f) Y_2CFCl Janus MXene monolayers. Solid and dashed lines show a comparison of exciton absorption and single particle absorption spectra, respectively.

dimensional materials, as it quantifies the strength of quasiparticle effects and their influence on the linear optical properties.

Unlike bulk (3D) systems, where excitonic effects can often be neglected, 2D materials exhibit significantly stronger electron−hole interactions due to reduced dielectric screening and quantum confinement in the nonperiodic direction. Consequently, binding energies in 2D semiconductors typically fall within the range of 100−500 meV,[52−55] often leading to a pronounced red shift in the optical absorption onset.

Moreover, the magnitude of E_b is highly sensitive to the surrounding dielectric environment, which can substantially reduce the binding energy relative to the vacuum condition considered in this work.[52] These effects modulate the excitonic spectrum and govern optical and electronic transitions and can be experimentally probed using one- and two-photon spectroscopic selection rules.[56,57]

The computed exciton binding energies for the investigated Janus MXene monolayers range from 249.47 to 372.64 meV. Among the studied configurations, Sc_2CFBr exhibits the lowest binding energy (249.47 meV), whereas Y_2CFCl shows the highest value (372.64 meV). Overall, Y_2CTT' monolayers tend to exhibit larger exciton binding energies compared to their Sc_2CTT' counterparts, indicating a stronger Coulombic electron−hole interaction in the yttrium-based systems.

These results are consistent with previous studies on other two-dimensional semiconductors.[52,55,58,59] The substantial electron−hole coupling observed here plays a central role in shaping the linear optical response of these materials, further reinforcing their potential for optoelectronic and photovoltaic applications.

The linear optical response, considering incident light polarized along the x (blue curves) and y (black curves) directions, is shown in Figure 5 in terms of the absorption coefficient.

To provide a comprehensive analysis, two types of calculations were performed: (i) the independent-particle approximation (IPA, dashed curves), which neglects electron−hole interactions, and (ii) the Bethe−Salpeter equation (BSE, solid curves), which explicitly accounts for excitonic effects. Both results are valuable for interpreting optical properties, as the red shift in the absorption onset due to quasiparticle interactions can vary depending on the dielectric environment. In practical scenarios in which the monolayer is integrated into an optoelectronic device, the effective optical response is expected to lie between the BSE and IPA predictions.

The optical absorption spectra of Sc_2CFBr and Sc_2CFCl monolayers are shown in Figure 5(b) and (c), respectively. As indicated in Table 4, these materials exhibit relatively large exciton binding energies, influencing the position of their optical absorption onsets.

Both systems display prominent absorption peaks within the visible region at the BSE level, highlighting their potential for applications in light-harvesting technologies. In contrast, under the IPA approximation, the main absorption features are

https://doi.org/10.1021/acsaem.5c00657
ACS Appl. Energy Mater. 2025, 8, 6634−6644

shifted toward the ultraviolet range due to the absence of electron−hole interactions.

This shift underscores the importance of incorporating many-body effects to predict the optical behavior accurately. The combination of strong visible-light absorption and significant excitonic effects suggests that Janus MXenes are promising candidates for photovoltaic and optoelectronic applications.[10,60]

For the Y_2CTT' Janus MXenes, lower excitonic band gaps are observed, as presented in Table 4 and illustrated in Figure 5(d−f), which correspond to the Y_2CClBr, Y_2CFBr, and Y_2CFCl monolayers, respectively. In the case of Y_2CClBr, the BSE-calculated absorption spectrum shows a pronounced peak at 1.54 eV in both the *x* and *y* polarization directions, placing the optical transition within the infrared region. In contrast, the dominant absorption features are shifted to the ultraviolet range at the IPA level due to the absence of excitonic corrections.

A similar infrared response is observed for Y_2CFBr and Y_2CFCl, where electron−hole interactions significantly lower the optical excitation threshold. These trends further highlight the crucial role of excitonic effects in modulating the optical properties of these materials.

These findings demonstrate the potential of Janus MXenes for infrared sensing, optoelectronic devices, and photovoltaic technologies, owing to their tunable optical and electronic characteristics.[61]

3.4. Power Conversion Efficiency. This section presents an analysis of the solar energy harvesting capabilities of Janus MXene monolayers, evaluated through their power conversion efficiency (PCE). Calculations were performed with and without excitonic effects using the BSE and IPA approaches, respectively.

The PCE is a key metric for assessing the photovoltaic potential of a material as it quantifies its ability to convert incident solar energy into electrical energy. To estimate the efficiency, we employed two widely used theoretical frameworks: the Shockley−Queisser (SQ) limit[42] and the spectroscopic limited maximum efficiency (SLME) method.[43]

Our analysis considers three levels of theoretical approximation: (i) the SLME-based power conversion efficiency (PCE^{SLME}), (ii) the maximum SLME efficiency assuming ideal phonon-assisted absorption from the band edge (PCE^{SLME}_{max}), and (iii) the SQ limit efficiency (PCE^{SQ}), which accounts only for radiative recombination losses under ideal semiconductor behavior.[42,62] The computed values under each model are listed in Tables S3−S5 of the Supporting Information.

To determine the PCE for the Janus MXenes, we incorporated both direct and indirect band gaps as well as excitonic ground-state transitions. These critical input parameters, including the direct exciton energy Ex_{gs}, are summarized in Table 4. The upper-efficiency limits were estimated using the following expression[11,52]

$$\mathrm{PCE} = \frac{J_{SC} V_{OC}}{P_{SOLAR}} \tag{2}$$

where V_{OC} represents the maximum open-circuit voltage, J_{SC} is the short-circuit current, and P_{SOLAR} is the total incident solar power per unit area. J_{SC} and P_{SOLAR} are defined as

$$J_{SC} = \int_{E_g^d}^{\infty} \frac{P(E)}{E}\, dE \tag{3}$$

and

$$P_{SOLAR} = \int_0^{\infty} P(E)\, dE \tag{4}$$

In this context, E_g^d denotes the electronic band gap of the donor material. In contrast, $P(E)$ corresponds to the AM1.5G solar spectral irradiance, the standard reference spectrum for photovoltaic conversion under nonconcentrated sunlight conditions.[44]

To account for excitonic effects in the PCE estimations, the electronic band gap was replaced by an optical band gap, defined by the energy of the direct excitonic ground state (Ex_{gs}). This modification offers a more realistic assessment of photovoltaic performance, particularly for two-dimensional semiconductors, where excitonic interactions significantly influence light absorption and charge carrier dynamics.

Figure 6a presents a bar chart comparing the power conversion efficiencies (PCE^{SLME}) computed at both the IPA and BSE levels. These calculations consider the atomic-scale thickness of the Janus MXene monolayers, which ranges from 8.52 Å to 9.52 Å (see Table 1). This ultrathin nature, typical of two-dimensional materials, leads to low optical absorbance—below 10%—and, consequently, reduced PCE values. At the IPA level, all predicted efficiencies remain below 1%, while including excitonic effects via the BSE approach raises the

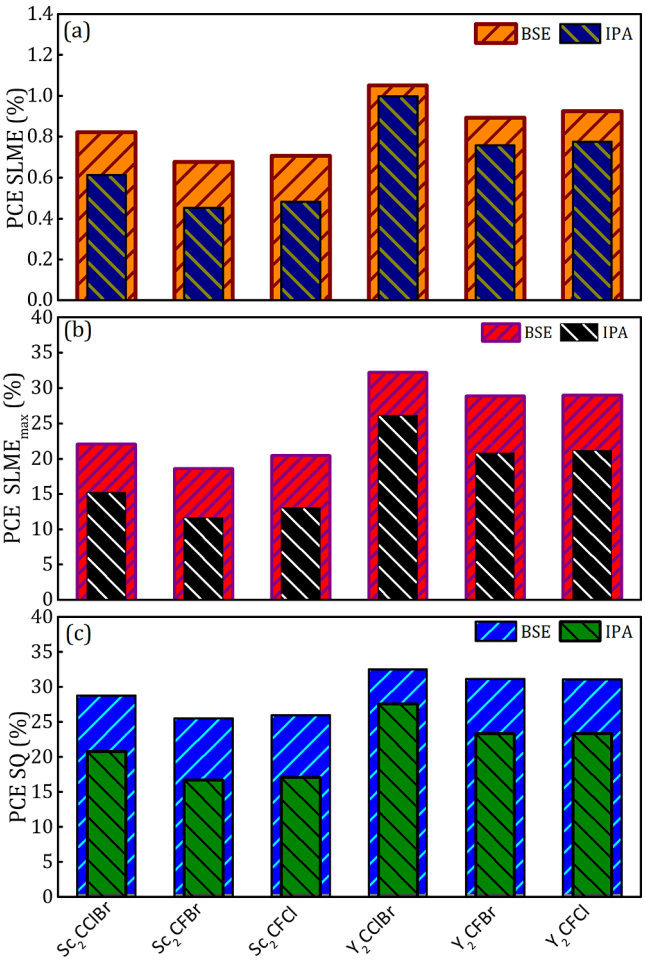

Figure 6. (a) PCE of SLME, (b) PCE $SLME_{MAX}$, and (c) PCE SQ for Sc_2CClBr, Sc_2CFBr, Sc_2CFCl, Y_2CClBr, Y_2CFBr, and Y_2CFCl Janus MXene monolayers.

https://doi.org/10.1021/acsaem.5c00657
ACS Appl. Energy Mater. 2025, 8, 6634−6644

efficiency above this threshold for some configurations. These differences highlight the significant impact of many-body effects on photovoltaic performance. Further details can be found in Figure S10 of the Supporting Information.

The maximum theoretical PCEs (PCE_{max}^{SLME}), as shown in Figure 6b, assume ideal light absorption starting at the band edge-conditions that could be approached in real devices through design optimizations and light trapping techniques.[63] Under these conditions, the BSE-level efficiencies increase substantially, ranging from 18.85% to 32.19%, whereas IPA-level values range from 11.61% to 26.09%. Notably, the Y_2CClBr monolayer demonstrates the highest performance, with a predicted efficiency of 32.19%. A complete data set for all calculated values is provided in Section S6 of the Supporting Information.

Finally, Figure 6c illustrates the Shockley–Queisser limit PCEs (PCE^{SQ}), which depend directly on the electronic band gap. As expected, these values exceeded those predicted by the SLME method. Again, Y_2CClBr exhibits the highest efficiency across all configurations. Under IPA, PCE^{SQ} values span from 16.74% to 27.61%, while the inclusion of excitonic effects via BSE increases this range to 25.52% to 32.57%. The discrepancy between SLME and SQ-based predictions is attributed to the recombination fraction (fr), defined as the energy difference between Ex_{gs}^{d} (BSE) and E_g^d (IPA). Because this difference is typically larger when excitonic effects are included, SLME-based PCE predictions tend to be lower at the BSE level than at the IPA level.

The estimated solar energy conversion efficiencies of Janus MXene monolayers underscore their strong promise for future photovoltaic technologies. Our predicted values, which approach the theoretical Shockley–Queisser limit, represent a meaningful step forward in the search for efficient, low-dimensional solar materials.

It is worth mentioning that the performance of these monolayers rivals, or even surpasses, that of several well-established photovoltaic systems, including SbSSe, CdTe, perovskites, GaInP, GaAs, and crystalline silicon (c-Si), as reported in previous studies.[62] These findings highlight Janus MXenes as compelling candidates for efficient solar energy harvesting and advanced optoelectronic applications.

4. CONCLUSIONS

In summary, we investigated the structural, electronic, and optoelectronic properties of six semiconducting Janus MXene monolayers—Sc_2CClBr, Sc_2CFBr, Sc_2CFCl, Y_2CClBr, Y_2CFBr, and Y_2CFCl, using DFT and a semiempirical MLWF-TB + BSE approach.

Our results confirm that all monolayers exhibit indirect band gaps, with HSE06 values ranging from 1.63 to 1.83 eV. The exciton binding energies further revealed strong electron–hole interactions, particularly in the Y_2TT' compounds, which reached up to 372.64 meV. These findings emphasize the key role of excitonic effects in determining the optical properties of these systems.

Optical absorption analysis showed that Sc_2TT' monolayers strongly absorb in the visible-light region. In contrast, Y_2TT' systems exhibit enhanced absorption in the infrared, particularly when excitonic effects are accounted for at the BSE level. These complementary spectral responses position Janus MXenes as promising materials for visible and IR optoelectronic devices.

Power conversion efficiency (PCE) calculations yielded Shockley–Queisser values approaching 31% under BSE, underscoring the photovoltaic potential of these low-dimensional materials for next-generation solar energy technologies.

■ ASSOCIATED CONTENT

Supporting Information

The Supporting Information is available free of charge at https://pubs.acs.org/doi/10.1021/acsaem.5c00657.

PAW projectors: computational technical details; structural data in the POSCAR format; thermodynamic properties; density of states; excitonic and optical properties simulation parameters; optical absorbance at IPA and BSE level, mechanical properties, Bader Charge Analysis, mathematical formalism for power conversion efficiency calculations, and insights of solar harvesting efficiency (PDF)

■ AUTHOR INFORMATION

Corresponding Authors

Bill D. Aparicio-Huacarpuma – *Institute of Physics and Computational Materials Laboratory, LCCMat, Institute of Physics, University of Brasília, 70919-970 Brasília, Brazil*; Email: bdaparicioh@gmail.com

Luiz Antônio Ribeiro Júnior – *Institute of Physics and Computational Materials Laboratory, LCCMat, Institute of Physics, University of Brasília, 70919-970 Brasília, Brazil*; orcid.org/0000-0001-7468-2946; Email: ribeirojr@unb.br

Authors

Marcelo Lopes Pereira Júnior – *University of Brasília, College of Technology, Department of Electrical Engineering, University of Brasília, 70910-900 Brasília, Brazil*; orcid.org/0000-0001-9058-510X

Alysson M. A. Silva – *College of Technology, Department of Mechanical Engineering, University of Brasília, 70910-900 Brasília, Brazil*

Alexandre C. Dias – *Institute of Physics and International Center of Physics, University of Brasília, 70919-970 Brasília, Brazil*

Complete contact information is available at: https://pubs.acs.org/10.1021/acsaem.5c00657

Funding

The Article Processing Charge for the publication of this research was funded by the Coordenacao de Aperfeicoamento de Pessoal de Nivel Superior (CAPES), Brazil (ROR identifier: 00x0ma614).

Notes

The authors declare no competing financial interest.

■ ACKNOWLEDGMENTS

B.D.A.-H. acknowledges the support of CAPES, a Brazilian funding agency, for the PhD scholarship. The authors gratefully acknowledge financial support from the following institutions: the National Council for Scientific and Technological Development (CNPq), the Federal District Research Support Foundation (FAPDF), and the Coordination for Improvement of Higher Education Personnel (CAPES). The authors also express their gratitude to the National Laboratory for Scientific Computing for providing resources through the

Santos Dumont supercomputer and to the Centro Nacional de Processamento de Alto Desempenho em São Paulo (CENAPAD-SP, UNICAMP/FINEP—MCTI project) for support related to project 897. Additional resources were provided by Lobo Carneiro HPC (NACAD) at the Federal University of Rio de Janeiro (UFRJ) for project 133. M.L.P.J. acknowledges financial support from the Research Support Foundation of the Federal District (FAPDF, grant 00193-00001807/2023-16) and the National Council for Scientific and Technological Development (CNPq, grant 444921/2024-9). A.C.D. acknowledges financial support from FAPDF grants 00193-00001817/2023-43 and 00193-00002073/2023-84 and CNPq grants 305174/2023-1, 444069/2024-0, and 444431/2024-1. L.A.R.J acknowledges financial support from FAPDF grant 0193.000942/2015, CNPq grants 307345/2021-1 and 350176/2022-1, and FAPDF-PRONEM grant 00193.00001247/2021-20. A.C.D. and L.A.R.J. also acknowledge funding from PDPG-FAPDF-CAPES Centro-Oeste grant number 00193-00000867/2024-94. This paper was published under the CC BY Open Access license through the ACS-CAPES agreement. The authors gratefully acknowledge CAPES for the financial support provided for the publication of this work under the ACS-CAPES agreement.

REFERENCES

(1) VahidMohammadi, A.; Rosen, J.; Gogotsi, Y. The world of two-dimensional carbides and nitrides (MXenes). *Science* **2021**, *372*, No. eabf1581.
(2) Khazaei, M.; Ranjbar, A.; Esfarjani, K.; Bogdanovski, D.; Dronskowski, R.; Yunoki, S. Insights into exfoliation possibility of MAX phases to MXenes. *Phys. Chem. Chem. Phys.* **2018**, *20*, 8579−8592.
(3) Gogotsi, Y.; Anasori, B. The Rise of MXenes. *ACS Nano* **2019**, *13*, 8491−8494.
(4) Kubitza, N.; Büchner, C.; Sinclair, J.; Snyder, R. M.; Birkel, C. S. Extending the Chemistry of Layered Solids and Nanosheets: Chemistry and Structure of MAX Phases, MAB Phases and MXenes. *ChemPlusChem* **2023**, *88*, 00214.
(5) Dahlqvist, M.; Petruhins, A.; Lu, J.; Hultman, L.; Rosen, J. Origin of Chemically Ordered Atomic Laminates (i-MAX): Expanding the Elemental Space by a Theoretical/Experimental Approach. *ACS Nano* **2018**, *12*, 7761−7770.
(6) Verger, L.; Natu, V.; Carey, M.; Barsoum, M. W. MXenes.: An Introduction of Their Synthesis, Select Properties, and Applications. *Trends Chem.* **2019**, *1*, 656−669.
(7) Zhou, A.; Liu, Y.; Li, S.; Wang, X.; Ying, G.; Xia, Q.; Zhang, P. From structural ceramics to 2D materials with multi-applications: A review on the development from MAX phases to MXenes. *J. Adv. Ceram.* **2021**, *10*, 1194−1242.
(8) Modi, N.; Naik, Y.; Khengar, S.; Jariwala, P.; Shah, D.; Thakor, P. Theoretical investigations of asymmetric functionalized Y2C-based MXene monolayers. *Solid State Commun.* **2023**, *372*, 115303.
(9) Akgenc, B. Intriguing of two-dimensional Janus surface-functionalized MXenes: An ab initio calculation. *Comput. Mater. Sci.* **2020**, *171*, 109231.
(10) Zhang, Y.; Sa, B.; Miao, N.; Zhou, J.; Sun, Z. Computational mining of Janus Sc2C-based MXenes for spintronic, photocatalytic, and solar cell applications. *J. Mater. Chem. A* **2021**, *9*, 10882−10892.
(11) Bernardi, M.; Palummo, M.; Grossman, J. C. Semiconducting Monolayer Materials as a Tunable Platform for Excitonic Solar. *Cells* **2012**, *6*, 10082−10089.
(12) Wei, X.; Yan, F.-G.; Shen, C.; Lv, Q.-S.; Wang, K.-Y. Photodetectors based on junctions of two-dimensional transition metal dichalcogenides. *Chin. Phys. B* **2017**, *26*, 038504.
(13) Khazaei, M.; Mishra, A.; Venkataramanan, N. S.; Singh, A. K.; Yunoki, S. Recent advances in MXenes: From fundamentals to applications. *Curr. Opin. Solid State Mater. Sci.* **2019**, *23*, 164−178.
(14) Xiong, K.; Cheng, Z.; Liu, J.; Liu, P.-F.; Zi, Z. Computational studies on functionalized Janus MXenes MM'CT2, (M, M' = Zr, Ti, Hf, M ≠ M'; T = − O, − F, − OH) photoelectronic properties and potential photocatalytic activities. *RSC Adv.* **2023**, *13*, 7972−7979.
(15) Wong, Z. M.; Deng, T.; Shi, W.; Wu, G.; Tan, T. L.; Yang, S.-W. High performance photocatalytic and thermoelectric two-dimensional asymmetrically ordered Janus-like MXene alloys. *Mater. Adv.* **2020**, *1*, 1176−1185.
(16) Sibhatu, A. k.; Teshome, T.; Akin-Ojo, O.; Yimam, A.; Asres, G. A. DFT investigation of the electronic and optical properties of hexagonal MX 2/ZrXO (M= W, Mo and X= S, Se) van der Waals heterostructures for photovoltaic solar cell application. *RSC Adv.* **2022**, *12*, 30838−30845.
(17) Pacheco, J. M.; Gueorguiev, G. K.; Martins, J. L. First-principles study of the possibility of condensed phases of endohedral silicon cage clusters. *Phys. Rev. B:Condens. Matter Mater. Phys.* **2002**, *66*, 033401.
(18) Gueorguiev, G. K.; Stafström, S.; Hultman, L. Nano-wire formation by self-assembly of silicon−metal cage-like molecules. *Chem. Phys. Lett.* **2008**, *458*, 170−174.
(19) Alhamada, T.; Azmah Hanim, M.; Jung, D.; Nuraini, A.; Hasan, W. W. A brief review of the role of 2D mxene nanosheets toward solar cells efficiency improvement. *Nanomaterials* **2021**, *11*, 2732.
(20) Du, C.-F.; Zhao, X.; Wang, Z.; Yu, H.; Ye, Q. Recent advanced on the MXene−organic hybrids: Design, synthesis, and their applications. *Nanomaterials* **2021**, *11*, 166.
(21) Yang, R.; Chen, X.; Ke, W.; Wu, X. Recent research progress in the structure, fabrication, and application of MXene-based heterostructures. *Nanomaterials* **2022**, *12*, 1907.
(22) Rahman, U. U.; Humayun, M.; Ghani, U.; Usman, M.; Ullah, H.; Khan, A.; El-Metwaly, N. M.; Khan, A. MXenes as emerging materials: synthesis, properties, and applications. *Molecules* **2022**, *27*, 4909.
(23) Bandaru, S.; Jastrzębska, A. M.; Birowska, M. Recent progress in thermoelectric MXene-based structures versus other. *2D materials* **2023**, *34*, 101902.
(24) Kresse, G.; Hafner, J. Ab initio Molecular Dynamics for Open-Shell Transition Metals. *Phys. Rev. B:Condens. Matter Mater. Phys.* **1993**, *48*, 13115−13118.
(25) Kresse, G.; Furthmüller, J. Efficient Iterative Schemes For *Ab Initio* Total-Energy Calculations Using a Plane-Wave Basis set. *Phys. Rev. B:Condens. Matter Mater. Phys.* **1996**, *54*, 11169−11186.
(26) Hohenberg, P.; Kohn, W. Inhomogeneous Electron Gas. *Phys. Rev.* **1964**, *136*, B864−B871.
(27) Kohn, W.; Sham, L. J. Self-Consistent Equations Including Exchange and Correlation Effects. *Phys. Rev.* **1965**, *140*, A1133−A1138.
(28) Blöchl, P. E. Projector augmented-wave method. *Phys. Rev. B:Condens. Matter Mater. Phys.* **1994**, *50*, 17953−17979.
(29) Kresse, G.; Joubert, D. From ultrasoft pseudopotentials to the projector augmented-wave method. *Phys. Rev. B:Condens. Matter Mater. Phys.* **1999**, *59*, 1758−1775.
(30) Perdew, J. P.; Yue, W. Accurate and simple density functional for the electronic exchange energy: Generalized gradient approximation. *Phys. Rev. B:Condens. Matter Mater. Phys.* **1986**, *33*, 8800−8802.
(31) Perdew, J. P. Generalized gradient approximations for exchange and correlation: A look backward and forward. *Phys. B* **1991**, *172*, 1−6.
(32) Cohen, A. J.; Mori-Sánchez, P.; Yang, W. Fractional charge perspective on the band gap in density-functional theory. *Phys. Rev. B:Condens. Matter Mater. Phys.* **2008**, *77*, 115123.
(33) Crowley, J. M.; Tahir-Kheli, J.; Goddard, W. A. Resolution of the Band Gap Prediction Problem for Materials. *Design* **2016**, *7*, 1198−1203.

https://doi.org/10.1021/acsaem.5c00657
ACS Appl. Energy Mater. 2025, 8, 6634−6644

(34) Heyd, J.; Scuseria, G. E.; Ernzerhof, M. Erratum: "Hybrid functionals based on a screened Coulomb potential" [J. Chem. Phys. 118, 8207 (2003)]. *J. Chem. Phys.* **2006**, *124*, 219906.
(35) Abolade, S. A.; Akinpelu, S. B.; Obada, D. O.; Kumar R, S.; Akande, A. Insights into the band gap anomalies of certain bismuth-based chalcogenides through ab initio calculations of structural and electronic properties. *Results Phys.* **2024**, *64*, 107891.
(36) Momma, K.; Izumi, F. VESTA: a three-dimensional visualization system for electronic and structural analysis. *J. Appl. Crystallogr.* **2008**, *41*, 653−658.
(37) Wang, V.; Xu, N.; Liu, J.-C.; Tang, G.; Geng, W.-T. VASPKIT.: A user-friendly interface facilitating high-throughput computing and analysis using VASP code. *Comput. Phys. Commun.* **2021**, *267*, 108033.
(38) Togo, A.; Tanaka, I. First principles phonon calculations in materials. *Scr. Mater.* **2015**, *108*, 1−5.
(39) Mostofi, A. A.; Yates, J. R.; Lee, Y.-S.; Souza, I.; Vanderbilt, D.; Marzari, N. wannier90: A tool for obtaining maximally-localised Wannier functions. *Comput. Phys. Commun.* **2008**, *178*, 685−699.
(40) Dias, A. C.; Silveira, J. F.; Qu, F. WanTiBEXOS: A Wannier based Tight Binding code for electronic band structure, excitonic and optoelectronic properties of solids. *Comput. Phys. Commun.* **2023**, *285*, 108636.
(41) Rozzi, C. A.; Varsano, D.; Marini, A.; Gross, E. K. U.; Rubio, A. Exact Coulomb cutoff technique for supercell calculations. *Phys. Rev. B:Condens. Matter Mater. Phys.* **2006**, *73*, 205119.
(42) Shockley, W.; Queisser, H. J. Detailed Balance Limit of Efficiency of p-n Junction Solar Cells. *J. Appl. Phys.* **1961**, *32*, 510−519.
(43) Yu, L.; Zunger, A. Identification of Potential Photovoltaic Absorbers Based on First-Principles Spectroscopic Screening of Materials. *Phys. Rev. Lett.* **2012**, *108*, 068701.
(44) ASTM-G173-03 *Standard Tables for Reference Solar Spectral Irradiances: Direct Normal and Hemispherical on 37 Degree Tilted Surface*; ASTM International: West Conshohocken, PA, 2012.
(45) Bernardi, M.; Palummo, M.; Grossman, J. C. Extraordinary Sunlight Absorption and One Nanometer Thick Photovoltaics Using Two-Dimensional Monolayer. *Materials* **2013**, *13*, 3664−3670.
(46) Sheng, X.-F.; Chen, S.; Kang, W.-B.; Fang, W.-Y. Monolayer XN2 (X Ti, Zr, Hf): Novel 2D materials with high stability, simultaneously high electron and hole mobilities from density functional theory. *Mater. Today Commun.* **2022**, *31*, 103313.
(47) Amirian, S.; Fatahi, N.; Naseri, M. Two-dimensional functionalized Y2CX2 (X = F, Cl, Br, I) MXene semiconductors for photovoltaic applications. *Mater. Today Commun.* **2025**, *42*, 111217.
(48) Cadelano, E.; Palla, P. L.; Giordano, S.; Colombo, L. Elastic properties of hydrogenated graphene. *Phys. Rev. B:Condens. Matter Mater. Phys.* **2010**, *82*, 235414.
(49) Zhu, S.-Y.; Li, Y.-Q.; Wang, X.-Y.; Tang, D.-S.; He, Q.-W.; Liu, C.; Liu, F.-C.; Wang, X.-C. Theoretical investigations of Sc2C based functionalized MXenes for applications in nanoelectromechanical systems. *Phys. E* **2023**, *145*, 115491.
(50) He, Y. The structural, electronic, elastic and thermodynamics properties of 2D transition-metal electride Y2C via first-principles calculations. *J. Alloys Compd.* **2016**, *654*, 180−184.
(51) Wang, X.; Chen, L.; Yuan, Z.; Rong, J.; Feng, J.; Muzammil, I.; Yu, X.; Zhang, Y.; Zhan, Z. DHQ-graphene: a novel two-dimensional defective graphene for corrosion-resistant coating. *J. Mater. Chem. A* **2019**, *7*, 8967−8974.
(52) Dias, A. C.; Bragança, H.; de Mendonça, J. P. A.; Da Silva, J. L. F. Excitonic Effects on Two-Dimensional Transition-Metal Dichalcogenide Monolayers: Impact on Solar Cell Efficiency. *ACS Appl. Energy Mater.* **2021**, *4*, 3265−3278.
(53) Wen, W.; Wu, L.; Yu, T. Excitonic Lasers in Atomically Thin 2D Semiconductors. *ACS Mater. Lett.* **2020**, *2*, 1328−1342.
(54) Raja, A.; Chaves, A.; Yu, J.; Arefe, G.; Hill, H. M.; Rigosi, A. F.; Berkelbach, T. C.; Nagler, P.; Schüller, C.; Korn, T.; Nuckolls, C.; Hone, J.; Brus, L. E.; Heinz, T. F.; Reichman, D. R.; Chernikov, A. Coulomb engineering of the bandgap and excitons in two-dimensional materials. *Nat. Commun.* **2017**, *8*, 15251.
(55) Cavalheiro Dias, A.; Almeida Cornélio, C. D.; Piotrowski, M. J.; Ribeiro Júnior, L. A.; de Oliveira Bastos, C. M.; Caldeira Rêgo, C. R.; Guedes-Sobrinho, D. Can. 2D Carbon Allotropes Be Used as Photovoltaic Absorbers in Solar Harvesting Devices? *ACS Appl. Energy Mater.* **2024**, *7*, 8572−8582.
(56) Barros, E. B.; Capaz, R. B.; Jorio, A.; Samsonidze, G. G.; Souza Filho, A. G.; Ismail-Beigi, S.; Spataru, C. D.; Louie, S. G.; Dresselhaus, G.; Dresselhaus, M. S. Selection rules for one- and two-photon absorption by excitons in carbon nanotubes. *Phys. Rev. B:Condens. Matter Mater. Phys.* **2006**, *73*, 241406.
(57) Attaccalite, C.; Grüning, M.; Amara, H.; Latil, S.; Ducastelle, F. Two-photon absorption in two-dimensional materials: The case of hexagonal boron nitride. *Phys. Rev. B:Condens. Matter Mater. Phys.* **2018**, *98*, 165126.
(58) Zhu, B.; Chen, X.; Cui, X. Exciton Binding Energy of Monolayer WS2. *Sci. Rep.* **2015**, *5*, 9218.
(59) Moujaes, E. A.; Dias, A. C. On the excitonic effects of the 1T and 1OT phases of PdS2, PdSe2, and PdSSe monolayers. *J. Phys. Chem. Solid.* **2023**, *182*, 111573.
(60) Zhang, R.-Z.; Ding, H.; Li, X.-H.; Cui, H.-L. Quantum capacitance, electronic and optical properties of Janus Sc2CXY (X = O, S, se, Te; Y = F, cl, Br, I) MXenes: First-principle investigation. *J. Energy Storage* **2025**, *108*, 115167.
(61) Yang, S.; Huang, W.; Lin, Z.; Chen, Z.; Yang, R.; Jia, Y.; Liu, X.; Wang, R.; Zeng, Z.; Hu, Y.; Chen, H.; Gui, X. Janus MXene film with gradient structure for highly efficient terahertz and infrared electromagnetic absorption. *Nano Res.* **2025**, *18*, 94907041.
(62) Ehrler, B.; Alarcón-Lladó, E.; Tabernig, S. W.; Veeken, T.; Garnett, E. C.; Polman, A. Photovoltaics Reaching for the Shockley−Queisser Limit. *Energy Lett.* **2020**, *5*, 3029−3033.
(63) Jariwala, D.; Davoyan, A. R.; Wong, J.; Atwater, H. A. Van der Waals Materials for Atomically-Thin Photovoltaics: Promise and Outlook. *ACS Photonics* **2017**, *4*, 2962−2970.

https://doi.org/10.1021/acsaem.5c00657
ACS Appl. Energy Mater. 2025, 8, 6634−6644